A Novel Balanced-to-Unbalanced All-Port Reflectionless Filtering Power Divider without Loading Additional Absorptive Branches at Input and Output Ports

Qi Chen[1], Huabin Zhang[1], Zhongbao Wang[1, 2, *], Hongmei Liu[1], and Shaojun Fang[1]

[1]*School of Information Science and Technology, Dalian Maritime University, Dalian, Liaoning 116026, China*
[2]*Liaoning Key Laboratory of Radio Frequency and Big Data for Intelligent Applications, Liaoning Technical University*
Huludao, Liaoning 125105, China

ABSTRACT: A novel balanced-to-unbalanced (BTU) all-port reflectionless filtering power divider without loading additional absorptive branches at input and output ports is proposed in this paper. The proposed power divider includes two reflectionless filtering networks, four transmission lines, a phase inverter, and two isolation resistors. Unlike the existing filtering power dividers that require additional absorptive branches to be loaded at each port to achieve reflectionlessness at all ports, the proposed power divider achieves all-port reflectionlessness by embedding only two reflectionless filtering networks in the BTU power dividing circuit. Meanwhile, this reflectionless filtering network also introduces two transmission zeros located at the lower and upper sides of the passband, respectively, for high selectivity. To validate the proposed power divider topology, a 2.0-GHz BTU filtering power divider is designed and fabricated with a 3-dB filtering bandwidth of 40.1%. The 10-dB reflectionless bandwidth for the balanced port is 98.7% from 0.940 to 2.772 GHz and that for the unbalanced ports covers the entire measurement frequency from 0.5 to 3.5 GHz, achieving good all-port reflectionless characteristics.

1. INTRODUCTION

In the fifth-generation (5G) era, various communication modes have become more complicated, and spectrum resources have become more precious. At the same time, in the field of RF systems, environmental noise, and electromagnetic interference present significant challenges, as they can greatly impair the performance of circuits and systems. How to improve the anti-interference capability of the system and maintain a certain signal-to-noise ratio under limited spectrum resources and high transmission rates has received widespread attention [1]. Subsequently, balanced circuits are becoming more widely used in RF and microwave systems because they have the advantages of high immunity to environmental noise, good common-mode suppression (CMS), and low electromagnetic interference, compared with the single-end counterparts. Due to these benefits, a large number of balanced circuits have been proposed, such as balanced filters [2–5], balanced amplifiers [6], and balanced mixers [7]. In addition, the balanced power dividers have been attracting more and more attention [8–11].

Balanced circuits are widely adopted due to their strong electromagnetic compatibility characteristics, while single-ended power dividers have the advantages of simple design and easy cascading. Therefore, the coexistence of balanced and unbalanced circuits in passive feeding networks is of great significance, and then, balanced-to-unbalanced (BTU) power dividers were proposed [12–17]. For integration of filtering function, a

filtering structure is typically employed in place of the conventional quarter-wavelength transmission line in a power divider. Several implementations of BTU filtering power dividers have been realized using coupled lines [15], the modified two-port coupled lines with short- and open-circuited stubs [16], and π-shaped network embedded with short-circuited stub [17]. When the aforementioned filtering power divider performs signal filtering, it allows in-band RF energy to be transmitted, while out-of-band RF energy is blocked and reflected back to the signal source, which may deteriorate the active stages in the RF front ends.

The reflectionless filter addresses the issues of conventional filters by effectively absorbing out-of-band signals through resistors and dissipating them as heat, reducing the energy returned by out-of-band signals and thereby improving the overall system performance [18–20]. Single-ended filters can achieve reflectionless capability by introducing resistor-loaded coupled-line structures [18] and band-stop filters [19] at their input and output ports. Recently, the concept of reflectionlessness has been applied to the design of single-ended filtering power dividers [21–24]. Based on the Wilkinson power divider, absorptive branches were loaded at input and output ports for realizing reflectionless characteristics [21]. In [22], two resistors and a resonator were added between the two output ports, which can provide an output reflectionless response. In [23], a synergistic absorptive stub that added at the input port and a composite T-type network were adopted to realize input reflectionless response. In [24], a single-ended narrowband filtering power divider was proposed that achieves reflectionless prop-

* Corresponding authors: Zhongbao Wang (wangzb@dlmu.edu.cn).

erty at the input and output ports by modifying the isolation network and adding resistor-loaded resonant networks at the output ports [24]. However, the additional absorptive branches and resistor-loaded resonant networks will increase the size of filtering power dividers. To the best of our knowledge, the BTU all-port reflectionless filtering power divider has not been reported before. Consequently, in order to solve the problems of differential input and all-port reflectionlessness of the above filtering power dividers, it is necessary to design a BTU filtering power divider with all-port reflectionless characteristics.

In this paper, a novel BTU all-port reflectionless filtering power divider is proposed. Unlike the aforementioned approach of loading absorptive branches at the input and output ports to achieve reflectionless response, the proposed BTU filtering power divider can achieve both all-port reflectionless and filtering function by embedding only two reflectionless filtering networks in the BTU power dividing circuit. Firstly, a novel reflectionless filtering network is proposed and analyzed. Then, the proposed reflectionless filtering network is applied to the BTU power dividing circuit, and the theoretical derivation for the circuit topology is performed. Lastly, simulated and measured results are given and discussed.

2. THEORY ANALYSIS AND DESIGN

Figure 1 depicts the schematic of the proposed BTU all-port reflectionless filtering power divider. The balanced differential input ports are defined by ports A+ and A−, and the two single-ended ports are ports 2 and 3 with impedance $Z_0 = 50\,\Omega$. This filtering power divider contains two novel reflectionless filtering networks (Block A), four transmission lines (Z_1, $\lambda/4$) and (Z_2, $\lambda/4$), a phase inverter (Z_3, $\lambda/2$), and two isolation resistors (R_2). The two reflectionless filtering networks are embedded in the BTU power dividing circuit to achieve the reflectionless performance of the inputs and outputs as well as the filtering function. Block A consists of a short-circuited stub (Z_a, $\lambda/4$), two open-circuited stubs (Z_b, $\lambda/4$), two transmission lines (Z_c, $\lambda/4$), two $\lambda/4$ coupled lines with the even- and odd-mode characteristic impedances of Z_e and Z_o, and two resistors (R_1).

The mixed-mode scattering matrix $\mathbf{S}_{mm}$ of the proposed BTU filtering power divider can be extracted from the standard scattering matrix $\mathbf{S}_{std}$ using the matrix conversion, and the mixed-mode scattering matrix $\mathbf{S}_{mm}$ can be expressed as [15]

$$\mathbf{S}_{mm} = \begin{bmatrix} S_{ddAA} & S_{dsA2} & S_{dsA3} & S_{dcAA} \\ S_{sd2A} & S_{ss22} & S_{ss23} & S_{sc2A} \\ S_{sd3A} & S_{ss32} & S_{ss33} & S_{sc3A} \\ S_{cdAA} & S_{csA2} & S_{csA3} & S_{ccAA} \end{bmatrix} \quad (1)$$

and

$$\begin{cases} S_{ddAA} = \frac{1}{2}\left(S_{A+A+} - S_{A+A-} - S_{A-A+} + S_{A-A-}\right) \\ S_{ccAA} = \frac{1}{2}\left(S_{A+A+} + S_{A+A-} + S_{A-A+} + S_{A-A-}\right) \\ S_{cdAA} = \frac{1}{2}\left(S_{A+A+} - S_{A+A-} + S_{A-A+} - S_{A-A-}\right) \\ S_{dcAA} = \frac{1}{2}\left(S_{A+A+} + S_{A+A-} - S_{A-A+} - S_{A-A-}\right) \end{cases} \quad (2)$$

$$\begin{cases} S_{sdnA} = \frac{1}{\sqrt{2}}\left(S_{nA+} - S_{nA-}\right) \\ S_{dsAn} = \frac{1}{\sqrt{2}}\left(S_{A+n} - S_{A-n}\right) \\ S_{scnA} = \frac{1}{\sqrt{2}}\left(S_{nA+} + S_{nA-}\right) \\ S_{csAn} = \frac{1}{\sqrt{2}}\left(S_{A+n} + S_{A-n}\right) \end{cases} \quad (3)$$

$$S_{ssij} = S_{ij} \quad (4)$$

where n, i, $j = 2$, 3, and the subscripts d, c, and s represent the differential mode (DM), common mode (CM), and single-ended ports, respectively. The mixed-mode scattering matrix $\mathbf{S}_{mm}$ of the proposed BTU filtering power divider is expected to satisfy the matching condition at both balanced and unbalanced ports, good isolation between the unbalanced output ports, excellent common-mode suppression, and equal power division. The following conditions should be met:

$$\begin{cases} S_{ddAA} = S_{dcAA} = S_{sc2A} = S_{sc3A} = 0 \\ S_{ss22} = S_{ss33} = S_{ss32} = S_{ss23} = 0 \\ |S_{sd2A}| = |S_{sd3A}| = \frac{1}{\sqrt{2}} \\ |S_{ccAA}| = 1 \end{cases} \quad (5)$$

In addition, due to the proposed BTU filtering power divider being symmetric along the symmetry line as shown in Figure 1, the analysis can be simplified by applying the odd- and even-mode equivalent circuits. To meet condition (5), the scattering matrixes $\mathbf{S}_o$ and $\mathbf{S}_e$ of the odd- and even-mode equivalent circuits can be expressed as [15]

$$\mathbf{S}_o = \begin{bmatrix} S_{oA+A+} & S_{oA+2} \\ S_{o2A+} & S_{o22} \end{bmatrix} = \begin{bmatrix} 0 & 2S_{A+2} \\ 2S_{2A+} & 0 \end{bmatrix} \quad (6)$$

$$\mathbf{S}_e = \begin{bmatrix} S_{eA+A+} & S_{eA+2} \\ S_{e2A+} & S_{e22} \end{bmatrix} = \begin{bmatrix} 2S_{A+A+} & 0 \\ 0 & 0 \end{bmatrix} \quad (7)$$

where the subscripts o and e denote the odd and even modes, respectively.

2.1. Analysis of the Proposed Reflectionless Filtering Network

Figure 2 shows the schematic of the proposed reflectionless filtering network, which can be analyzed in odd and even modes since it is symmetric along the center. The odd-mode equivalent circuit of the proposed reflectionless filtering network is shown in Figure 3(a). According to microwave network and circuit theory, the odd-mode input impedance Z_{ino} at port 1 is

$$Z_{ino} = \frac{A_{oo}Z_{TL1} + B_{oo}}{C_{oo}Z_{TL1} + D_{oo}} \quad (8)$$

where A_{oo}, B_{oo}, C_{oo}, and D_{oo} are the ABCD parameters of parallel coupled lines in Figure 3(a), which can be calculated according to [25]

$$\begin{bmatrix} A_{oo} & B_{oo} \\ C_{oo} & D_{oo} \end{bmatrix} = \begin{bmatrix} \frac{2(\cos^2\theta+1)-\sin^2\theta\left(\frac{Z_e}{Z_o}+\frac{Z_o}{Z_e}\right)}{4\cos\theta} & \mathrm{j}\frac{(Z_e+Z_o)\sin\theta}{2} \\ \mathrm{j}\frac{(Z_e+Z_o)\sin\theta}{2Z_eZ_o} & \cos\theta \end{bmatrix} \quad (9)$$
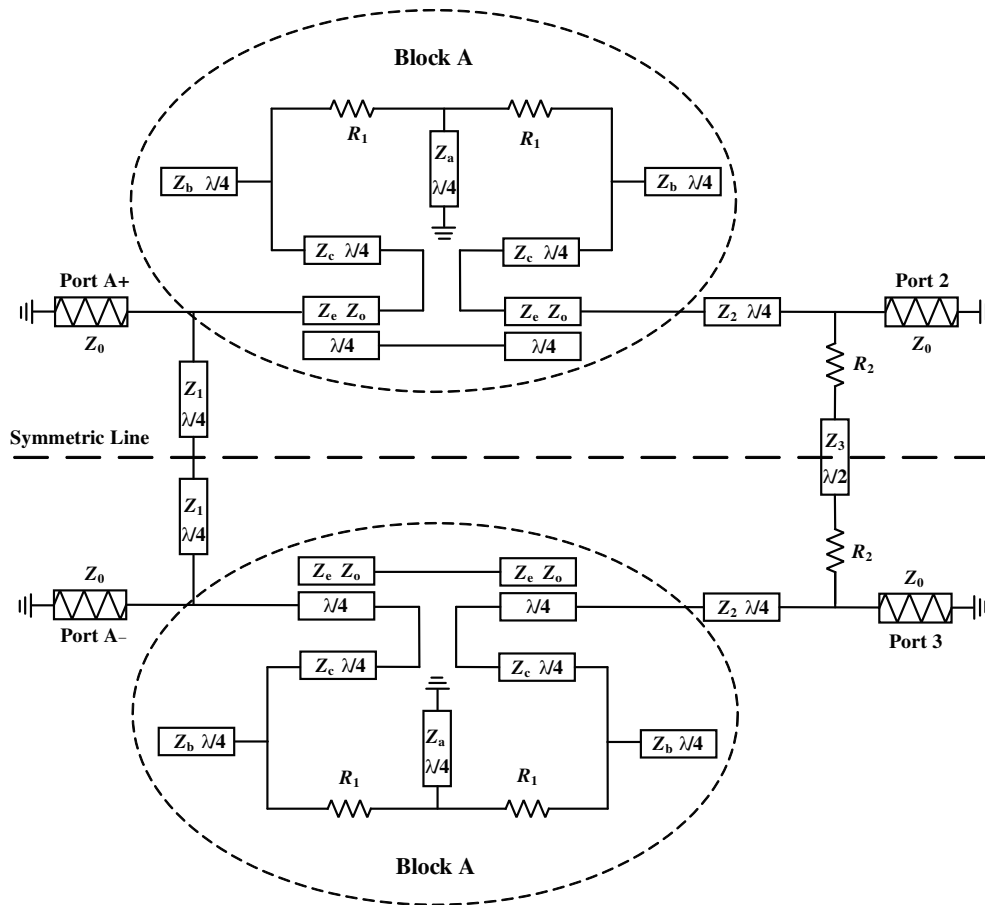
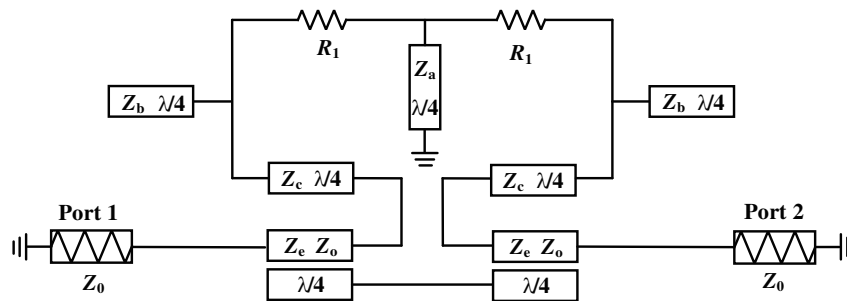**FIGURE 1**. Schematic of the proposed BTU all-port reflectionless filtering power divider.

FIGURE 2. Schematic of the proposed reflectionless filtering network (Block A).

At the same time, the Z_{TL1} and Z_{TL2} can be calculated as

$$Z_{\text{TL1}} = \frac{Z_c \left(Z_{\text{TL2}} + jZ_c \tan \theta\right)}{Z_c + jZ_{\text{TL2}} \tan \theta} \tag{10}$$

$$Z_{\text{TL2}} = \frac{Z_b R_1}{Z_b + jR_1 \tan \theta} \tag{11}$$

$$\theta = \frac{\pi f}{2 f_0} \tag{12}$$

where f_0 is the center frequency.

Similarly, referring to Figure 3(b) for even-mode analysis of the proposed reflectionless filtering network, the even-mode in-put impedance Z_{ine} at port 1 is

$$Z_{\text{ine}} = \frac{A_{\text{ee}} Z_{\text{TL3}} + B_{\text{ee}}}{C_{\text{ee}} Z_{\text{TL3}} + D_{\text{ee}}} \tag{13}$$

where A_{ee}, B_{ee}, C_{ee}, and D_{ee} are the *ABCD* parameters of parallel coupled lines in Figure 3(b).

$$\begin{bmatrix} A_{\text{ee}} & B_{\text{ee}} \\ C_{\text{ee}} & D_{\text{ee}} \end{bmatrix} = \begin{bmatrix} \cos \theta & j\frac{(Z_e + Z_o) \sin \theta}{2} \\ j\frac{2 \sin \theta}{Z_e + Z_o} & \cos \theta \end{bmatrix} \tag{14}$$

$$Z_{\text{TL3}} = \frac{Z_c \left(Z_{\text{TL4}} + jZ_c \tan \theta\right)}{Z_c + jZ_{\text{TL4}} \tan \theta} \tag{15}$$

$$Z_{\text{TL4}} = \frac{Z_b(R_1 + j2Z_a \tan \theta)}{Z_b + j(R_1 + j2Z_a \tan \theta) \tan \theta} \tag{16}$$
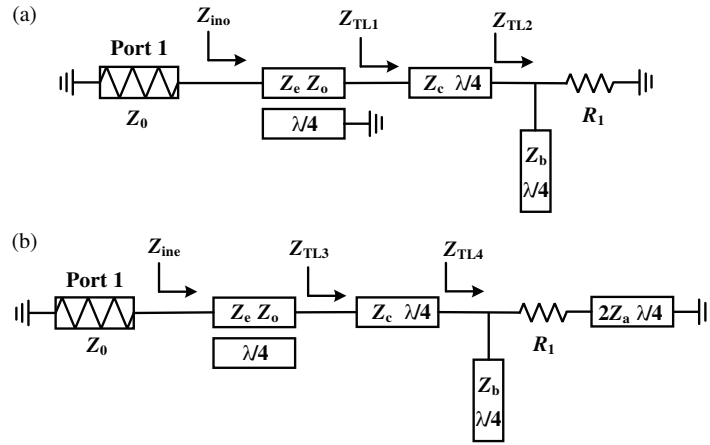
(a)

(b)

FIGURE 3. Equivalent circuits of the proposed reflectionless filtering network. (a) Odd mode. (b) Even mode.
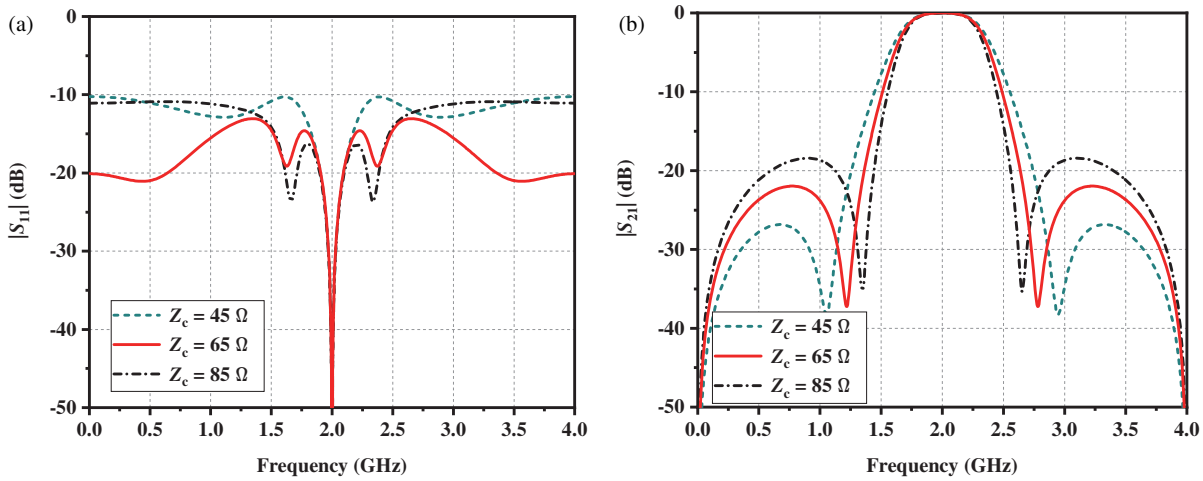
(a)

(b)

FIGURE 4. Effects of the Z_c on the S-parameters of the proposed reflectionless filtering network. (a) $|S_{11}|$. (b) $|S_{21}|$.

Based on the decomposition circuits in Figure 3, the S-parameter of the proposed reflectionless filtering network can be expressed as

$$S_{11} = S_{22} = \frac{Z_{\text{ine}} Z_{\text{ino}} - Z_0^2}{(Z_{\text{ine}} + Z_0)(Z_{\text{ino}} + Z_0)} \quad (17)$$

$$S_{21} = S_{12} = \frac{Z_{\text{ine}} Z_0 - Z_{\text{ino}} Z_0}{(Z_{\text{ine}} + Z_0)(Z_{\text{ino}} + Z_0)} \quad (18)$$

To meet the requirement of impedance matching (i.e., $S_{11} = 0$), the following relationship can be obtained as

$$(Z_e - Z_o)^2 \left(\frac{Z_e + Z_o}{4} + \frac{Z_o^2}{2Z_b} \right) (Z_c + Z_b) = Z_0^2 Z_c^2 \quad (19)$$

Therefore, the values of Z_e, Z_o, Z_b, and Z_c should be appropriately selected to satisfy impedance matching.

In order to control the location of the transmission zeros of the proposed reflectionless filter network, three cases for different Z_c are given in Table 1, where Z_b is calculated by using (19) with chosen $Z_e = 69.3\,\Omega$ and $Z_o = 23.0\,\Omega$ for obtaining ideal impedance matching at the center frequency; Z_a is tuned

to obtain the two transmission zeros near the pass band; and R_1 is tuned to obtain the reflectionless characteristics. Figure 4 gives the effect of Z_c on the S-parameters of the proposed reflectionless filtering network with the electrical parameters in Table 1. It can be found from Figure 4 that as Z_c increases from 45 to 85 Ω, the two transmission zeros move towards the passband, and the 3-dB filtering bandwidth slightly decreases. Therefore, the location of the two transmission zeros of the proposed reflectionless filter network can be controlled by Z_c.

Usually, the coupling coefficient k of coupled lines is defined as $k = (Z_e - Z_o)/(Z_e + Z_o)$. To analyze the effect of the coupling coefficient k on the S-parameters of the proposed reflectionless filtering network, three cases for different k are given in Table 2, where Z_c is tuned to fix the location of the two transmission zeros, then Z_b is calculated by using (19) with chosen Z_c and $\sqrt{Z_e Z_o} = 46.3\,\Omega$ for obtaining ideal impedance matching at the center frequency; Z_a is tuned to obtain the two transmission zeros near the pass band; and R_1 is tuned to obtain the reflectionless characteristics. Figure 5 gives the effect of the coupling coefficient k on the S-parameters of the proposed reflectionless filtering network with the electrical parameters
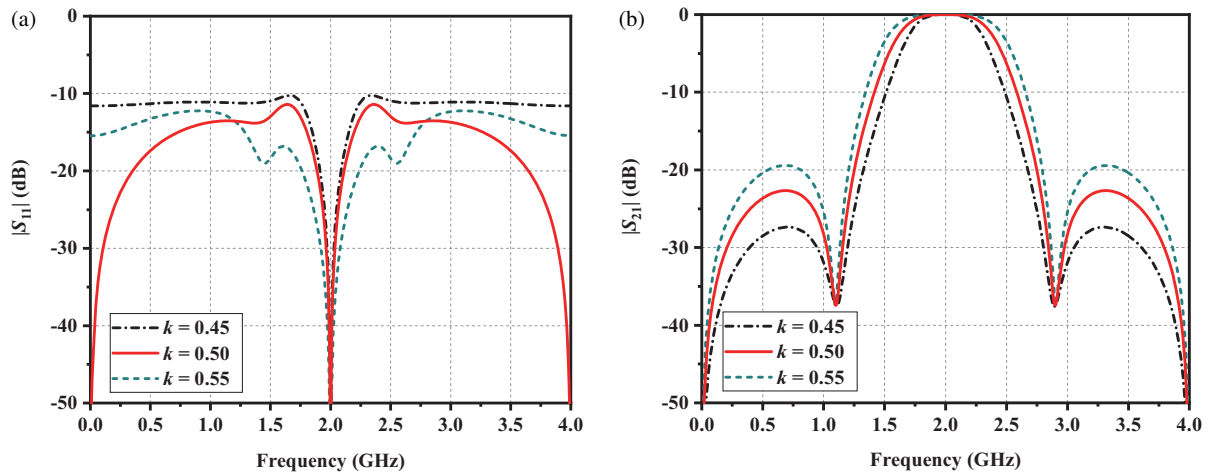
FIGURE 5. Effects of the coupling coefficient k on the S-parameters of the proposed reflectionless filtering network. (a) $|S_{11}|$. (b) $|S_{21}|$.
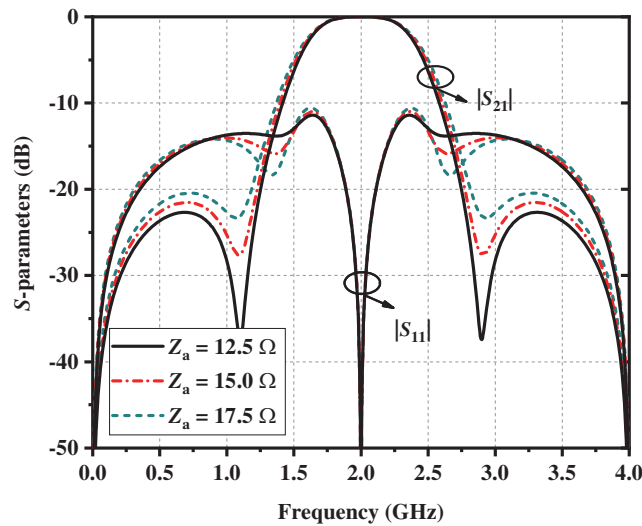

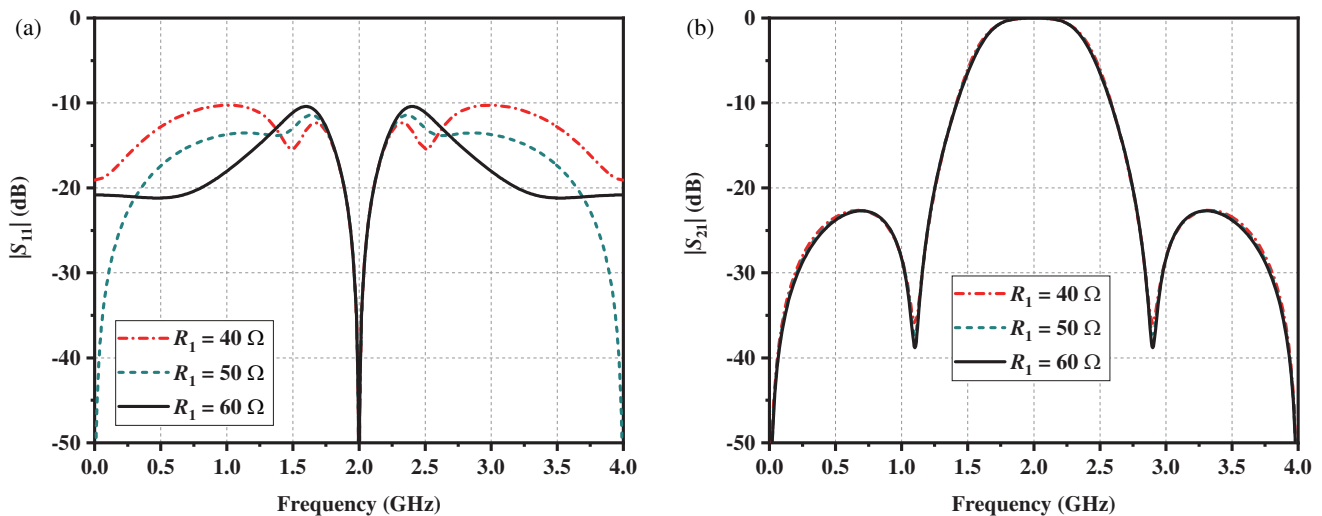**FIGURE 6**. Effects of the Z_a on the S-parameters of the proposed reflectionless filtering network.

FIGURE 7. Effects of the R_1 on the S-parameters of the proposed reflectionless filtering network. (a) $|S_{11}|$. (b) $|S_{21}|$.
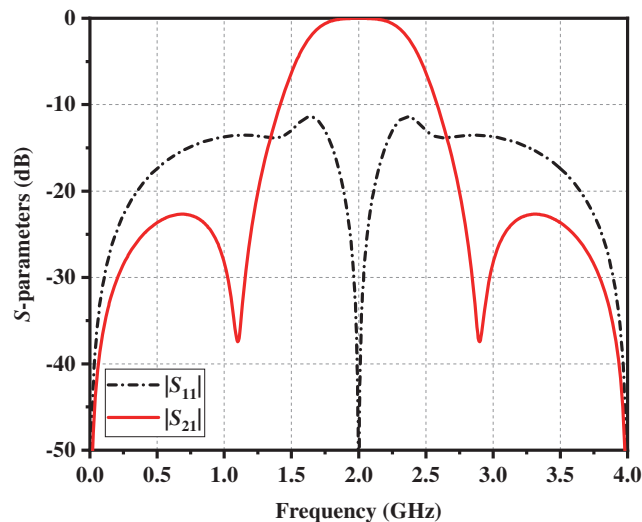
161

FIGURE 8. Simulation results of the proposed reflectionless filtering network.
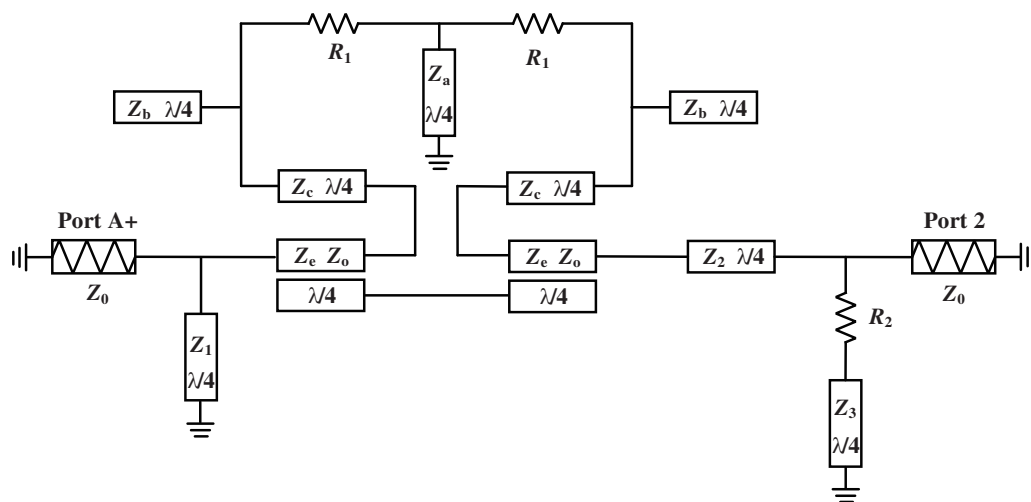

FIGURE 9. Odd-mode equivalent circuit of the proposed BTU all-port reflectionless filtering power divider.

TABLE 1. Electrical parameters for different Z_c with $Z_e = 69.3\,\Omega$ and $Z_o = 23.0\,\Omega$.

Z_c (Ω)	Z_a (Ω)	Z_b (Ω)	R_1 (Ω)
45	4.6	52.1	26.5
65	9.5	131.9	41.0
85	18.1	265.3	88.7

in Table 2. It can be seen from Figure 5 that as the coupling coefficient k increases, the 3-dB filtering bandwidth increases. Therefore, the bandwidth of the proposed reflectionless filtering network can be controlled by the coupling coefficient k of coupled lines used in it.

Figure 6 shows the effect of Z_a on the S-parameters of the proposed reflectionless filtering network. It can be seen that with the decrease of Z_a from 17.5 to 12.5 Ω, the out-of-band suppression improves, and two transmission zeros can be obtained. Therefore, the out-of-band filtering performance of the proposed reflectionless filtering network can be controlled by Z_a.

Figure 7 shows the effect of the absorption resistor R_1 on the S-parameters of the proposed reflectionless filtering network. It can be seen that as the R_1 increases from 40 to 60 Ω, the $|S_{11}|$ near 1 GHz and 3 GHz improves, but that near 1.5 GHz and 2.5 GHz becomes worse. Therefore, a trade-off reflectionless response can be obtained by tuning the R_1, which has negligible impact on $|S_{21}|$.

Figure 8 gives the simulation results of the proposed reflectionless filtering network with $Z_e = 79.6\,\Omega$, $Z_o = 27.0\,\Omega$, $Z_a = 11.5\,\Omega$, $Z_b = 110.0\,\Omega$, $Z_c = 80.5\,\Omega$, and $R_1 = 50\,\Omega$. As can be seen from Figure 8, the return loss is greater than 10 dB (i.e., $|S_{11}| < -10$ dB) at all frequencies from 0 to 4 GHz,
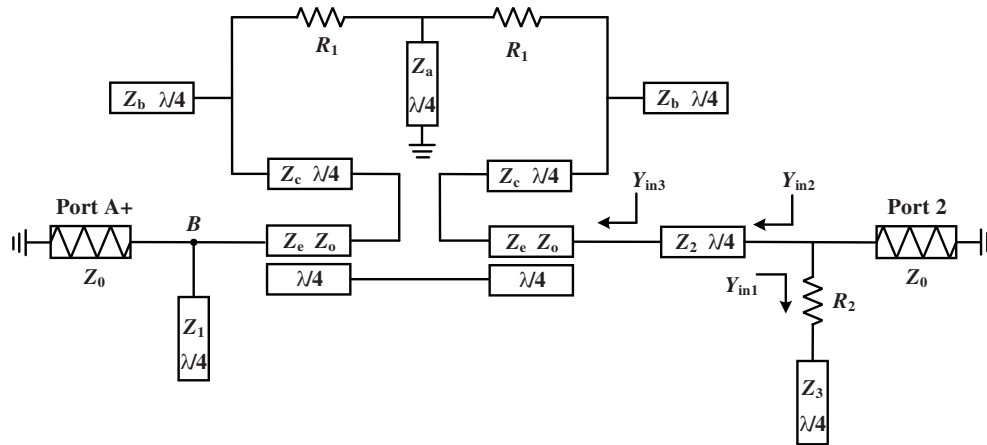
FIGURE 10. Even-mode equivalent circuit of the proposed BTU all-port reflectionless filtering power divider.
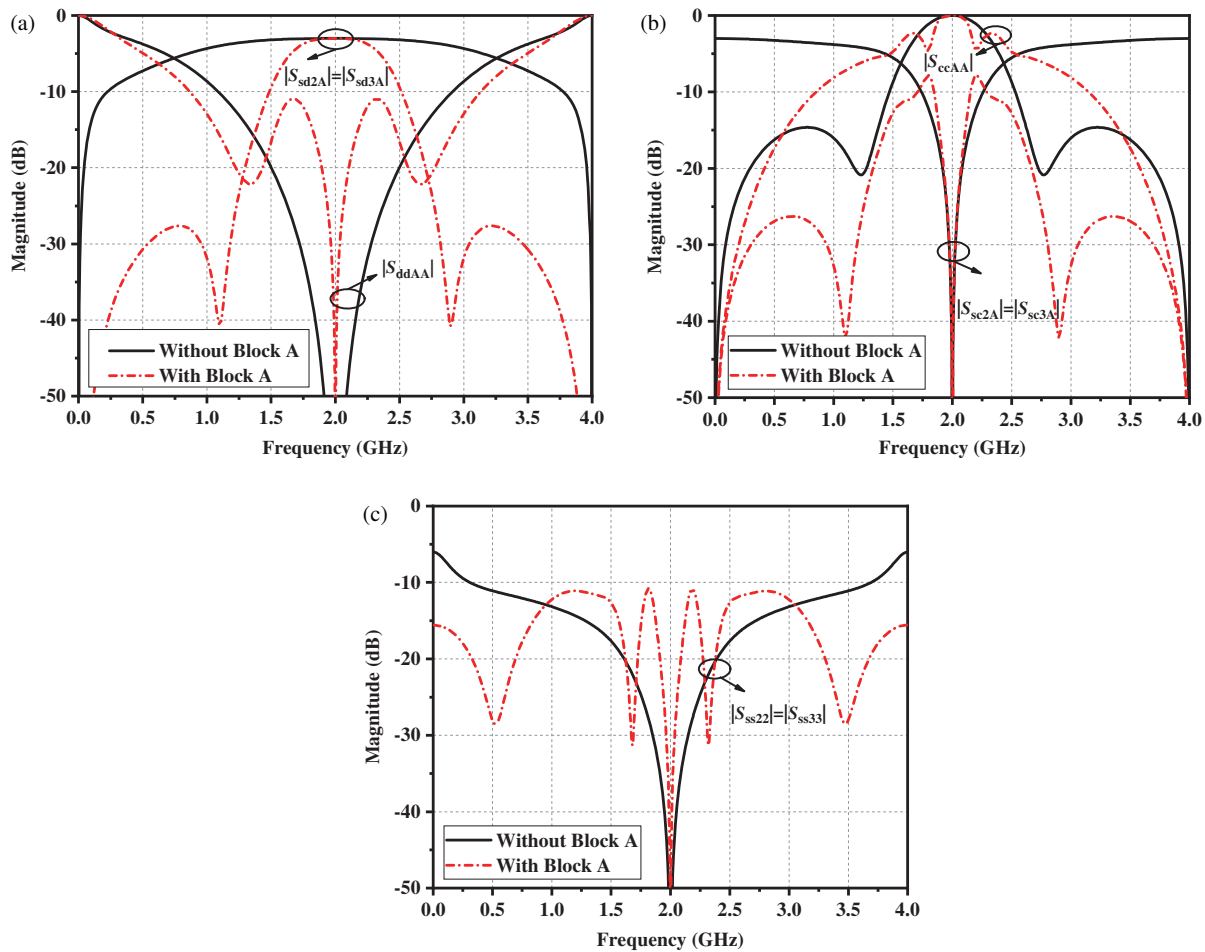

FIGURE 11. Simulation results of the proposed BTU power divider with and without Block A. (a) DM responses. (b) CM responses. (c) Unbalanced-port responses.

achieving wideband reflectionless characteristics. Transmission coefficient $|S_{21}|$ introduces two transmission zeros at 1.10 and 2.90 GHz, respectively, with a 3-dB filtering bandwidth of 40% ($1.6 \sim 2.4$ GHz) and the out-of-band rejection of better than 20 dB, achieving the filtering function. According to the transformation relationship between the S matrix and $ABCD$ matrix, the $ABCD$ matrix of the reflectionless filtering network

at the center frequency can be obtained as follows.

$$
\begin{bmatrix} A_1 & B_1 \\ C_1 & D_1 \end{bmatrix} = \begin{bmatrix} \frac{1}{2} & 0 \\ 0 & \frac{1}{2} \end{bmatrix} \tag{20}
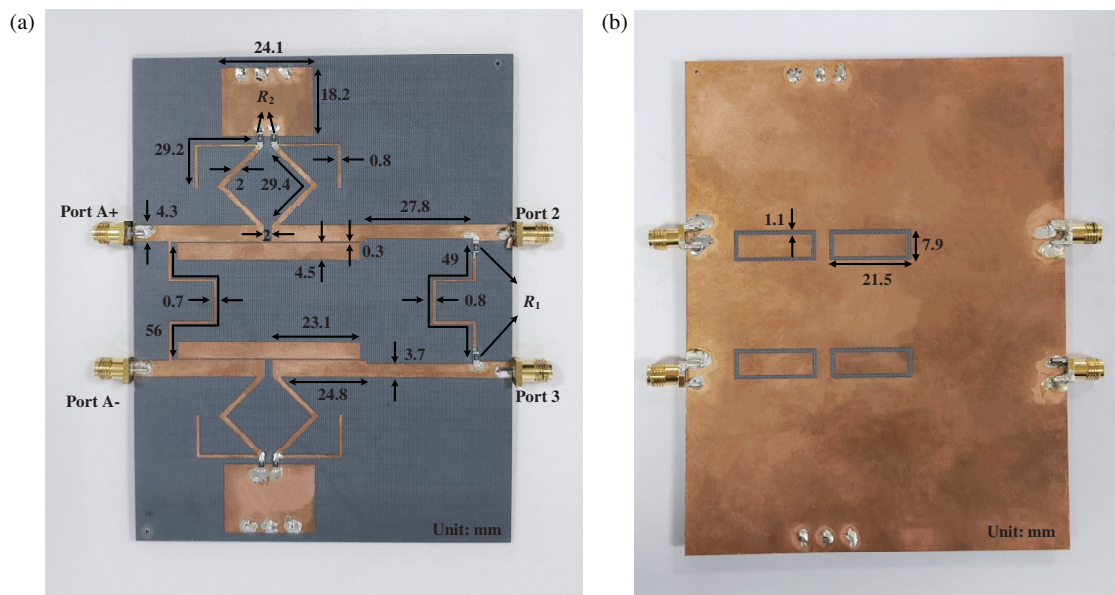$$

FIGURE 12. Photographs of the fabricated BTU all-port reflectionless filtering power divider. (a) Top view. (b) Bottom view.

TABLE 2. Electrical parameters for different coupling coefficients.

k	Z_e (Ω)	Z_o (Ω)	Z_a (Ω)	Z_b (Ω)	Z_c (Ω)	R_1 (Ω)
0.45	75.1	28.5	5.0	75.1	55.0	29.2
0.50	80.1	26.7	12.9	110	80.8	50.0
0.55	85.9	24.9	23.2	142	105	70.3

2.2. Analysis of the Proposed BTU Filtering Power Divider

When the odd-mode (i.e., differential-mode) signals are excited from ports A+ and A−, a virtual short-circuited wall appears along the symmetry line in Figure 1, and the odd-mode equivalent circuit is obtained and given in Figure 9. The $ABCD$ matrix between ports A+ and 2 of the odd-mode equivalent circuit can be calculated as

$$\begin{bmatrix} A & B \\ C & D \end{bmatrix} = \begin{bmatrix} 1 & 0 \\ \frac{1}{jZ_1 \tan\theta} & 1 \end{bmatrix} \begin{bmatrix} A_1 & B_1 \\ C_1 & D_1 \end{bmatrix}$$

$$\begin{bmatrix} \cos\theta & jZ_2\sin\theta \\ \frac{j\sin\theta}{Z_2} & \cos\theta \end{bmatrix} \begin{bmatrix} 1 & 0 \\ \frac{1}{R_2 + jZ_3\tan\theta} & 1 \end{bmatrix} \quad (21)$$

where $\begin{bmatrix} A_1 & B_1 \\ C_1 & D_1 \end{bmatrix}$ is the $ABCD$ matrix of the proposed re-

flectionless filtering network shown in Figure 2.

After $ABCD$-parameter to S-parameter transformations, according to (6), in order to satisfy $S_{oA+A+} = 0$, it can be obtained

$$Z_2 = Z_0 \quad (22)$$

When the even-mode (i.e., common-mode) signals are excited from ports A+ and A−, a virtual open-circuited wall appears along the symmetry line in Figure 1, and the even-mode equivalent circuit is obtained and given in Figure 10. Due to the $\lambda/4$ transmission line property, node B in Figure 10 can be

regarded as an ideal short-circuited point at f_0. Y_{in1} and Y_{in2} can be derived as

$$Y_{in1} = \frac{1}{R_2 - jZ_3\cot\theta} \quad (23)$$

$$Y_{in2} = Y_2 \frac{Y_{in3} + jY_2\tan\theta}{Y_2 + jY_{in3}\tan\theta} \quad (24)$$

$$Y_{in3} = \frac{D_1}{B_1} \quad (25)$$

Since $S_{e22} = 0$ in accordance with (7), to meet the port matching, the following equation should be satisfied:

$$Y_{in1} + Y_{in2} = Y_0 = \frac{1}{Z_0} \quad (26)$$

Combining (20) and (23)–(26), the following condition can be derived:

$$R_2 = Z_0 \quad (27)$$

Figure 11 shows the simulation results of the proposed BTU power divider with and without Block A (i.e., the proposed reflectionless filtering network). The BTU power divider with Block A introduces two reflection zeros at 1.33 and 2.67 GHz, widening the bandwidth for $|S_{ddAA}| < -10$ dB. Also, Block A introducing two transmission zeros at 1.10 GHz and 2.90 GHz has improved filtering selectivity, and out-of-band rejection of more than 20 dB has been obtained. Similarly, since Block A
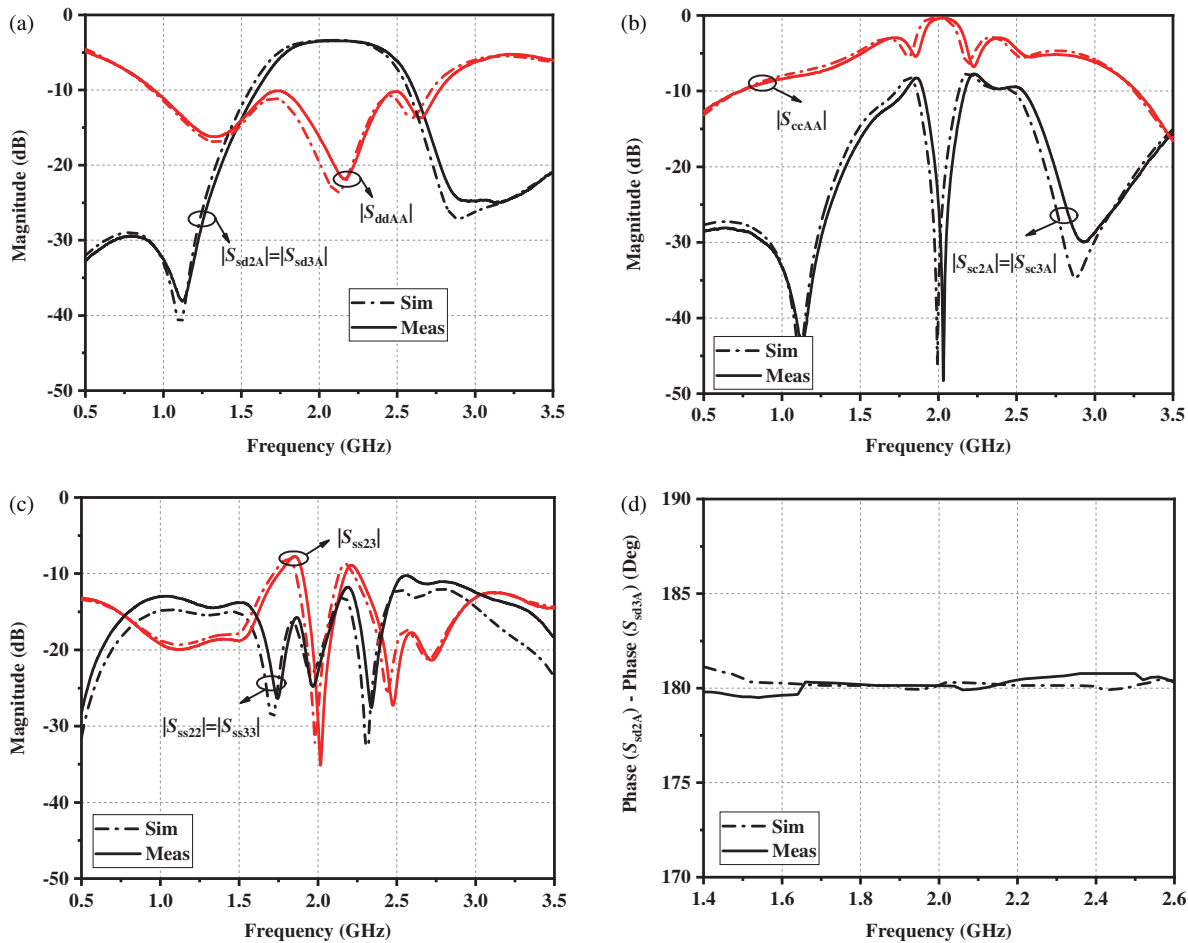
FIGURE 13. Simulation and measurement results of the proposed BTU all-port reflectionless filtering power divider (a) DM responses. (b) CM responses. (c) Unbalanced-port responses. (d) Phase difference.

also generates additional reflected zeros at the output ports, the matching bandwidths of the unbalanced ports are improved, achieving reflectionless characteristics of the output ports at the full frequency range from 0 to 4 GHz. At the same time, the common-mode rejection level has been improved to below -8.5 dB at all frequencies.

2.3. Design Procedure

Based on the above discussions and analysis, a simple design procedure of the proposed BTU all-port reflectionless filtering power divider can be summarized as follows.

1) Determine the desired center frequency f_0, the location of the transmission zeros, and bandwidth.

2) Select the value of Z_c based on the location of the transmission zeros, referring to Figure 4 and Table 1.

3) Select the values of Z_o and Z_e (i.e., coupling coefficient k) of the coupled lines based on the filtering bandwidth, referring to Figure 5 and Table 2.

4) Calculate the value of Z_b with Equation (19) for obtaining ideal impedance matching at the center frequency.

5) Adjust Z_a to obtain two transmission zeros near the passband and improve out-of-band suppression, referring to Figure 6.

6) Tune the absorption resistance R_1 to obtain the desired reflectionless response, referring to Figure 7.

7) Calculate the values of Z_2 and R_2 with Equations (22) and (27) to obtain the ideal input/output impedance matching characteristics at f_0, when the reflectionless filtering network is embedded in the BTU power divider.

8) The electrical parameters are further optimized with the ADS circuit simulator for better differential- and common-mode responses of the BTU filtering power divider, and the physical dimensions are optimized with the full-wave electromagnetic simulator.

3. IMPLEMENTATION AND PERFORMANCE

For validation, a BTU all-port reflectionless filtering divider with a center frequency of 2 GHz and 3-dB filtering bandwidth of 40% is designed, fabricated, and measured. Based on the previous analyses, the values of the electrical parameters obtained are shown in Table 3. The needed parallel coupled line with low odd-mode impedance and strong coupling is realized by using a defected ground [26]. The designed BTU power divider is realized with microstrip lines and fabricated on an F4B substrate with a thickness of 1.5 mm, a dielectric constant of 2.65, and a loss tangent of 0.003. After optimization by An-

TABLE 3. Electrical parameters of the proposed BTU all-port reflectionless filtering power divider.

Z_e (Ω)	Z_o (Ω)	Z_1 (Ω)	Z_2 (Ω)	Z_a (Ω)	Z_b (Ω)	Z_c (Ω)	R_1 (Ω)	R_2 (Ω)
79.6	27.0	110	50	11.5	110	80.5	50	50

TABLE 4. Comparisons between the proposed BTU filtering power divider and previous works.

Reference	Type	f_0 (GHz)	FBW (%)	CMS (dB)	Isolation (dB)	Reflectionless at input port	Reflectionless at output port	Loading additional absorptive branches
[16]	BTU	2.0	28.5	15	20	No	No	-
[17]	BTU	1.88	6.3	24	18	No	No	-
[21]	Single-ended	2.0	8.0	-	20	Yes	Yes	Yes
[22]	Single-ended	1.0	15.0	-	18	No	Yes	Yes
[23]	Single-ended	2.36	52.8	-	16	Yes	No	Yes
[24]	Single-ended	2.0	5.0	-	43	Yes	Yes	Yes
This work	BTU	2.0	40.1	30.4	28.5	Yes	Yes	No

soft HFSS software, the final dimensions and photographs are shown in Figure 12. The fabricated prototype is tested using an Agilent N5230A network analyzer.

Simulated and measured results of the proposed BTU all-port reflectionless filtering power divider are given in Figure 13. For the balanced-port DM responses, the differential-mode return loss is greater than 10 dB (i.e., $|S_{ddAA}| < -10$ dB) from 0.940 to 2.772 GHz (the 10-dB reflectionless bandwidth for the balanced port is 98.7%), achieving balanced-port reflectionless characteristics shown in Figure 13(a). In addition, the measured 3-dB filtering bandwidth (FBW) of the DM to 2-port (3-port) transmission coefficient $|S_{sd2A}|$ ($|S_{sd3A}|$) is 40.1% from 1.715 to 2.516 GHz. Two transmission zeros are achieved at 1.12 and 2.96 GHz, respectively, improving the filtering performance. For the balanced-port CM responses, the measured CM to 2-port (3-port) transmission coefficient $|S_{sc2A}|$ ($|S_{sc3A}|$) is less than -10 dB from 1.891 to 2.167 GHz with the center-frequency CMS of 30.4 dB, as shown in Figure 13(b). For the unbalanced-port responses, the single-ended return loss $|S_{ss22}|$ ($|S_{ss33}|$) is less than -10 dB at all frequencies, achieving unbalanced-port wideband reflectionless characteristics shown in Figure 13(c). In the frequency range from 1.90 to 2.18 GHz, the measured $|S_{ss23}|$ is less than -10 dB with the center-frequency isolation of 28.5 dB. As shown in Figure 13(d), the measured and simulated phase differences between the output ports 2 and 3 are $180° \pm 1°$ from 1.4 to 2.6 GHz, achieving wideband anti-phase output characteristics.

The comparisons between the proposed BTU filtering power divider and previous works are given in Table 4. This work is the first design of the BTU all-port reflectionless filtering power divider. Compared with the reported filtering power divider, the proposed BTU filtering power divider has a wide filtering bandwidth and good CM noise suppression. Furthermore, the reflectionless characteristics for all ports are obtained without loading additional absorptive branches at input and output ports.

4. CONCLUSION

In this paper, a novel BTU filtering power divider with all-port reflectionless characteristics has been presented. Unlike the existing filtering power dividers that require additional absorptive branches to be loaded at each port to achieve reflectionlessness at all ports, the proposed BTU filtering power divider achieves all-port reflectionlessness by embedding only two reflectionless filtering networks in the BTU power dividing circuit. Meanwhile, this reflectionless filtering network also introduces two transmission zeros located at the lower and upper sides of the passband, respectively, for high selectivity. The design equations of the proposed reflectionless filtering network and BTU filtering power divider have been derived for easy design. Besides, compared with the existing filtering power dividers, the proposed BTU filtering power divider has the advantages of DM signal transmission, good CMS, all-port reflectionless filtering, and wideband anti-phase output characteristics.

ACKNOWLEDGEMENT

REFERENCES

[1] Mahon, S., "The 5G effect on RF filter technologies," *IEEE Transactions on Semiconductor Manufacturing*, Vol. 30, No. 4, 494–499, Nov. 2017.

[2] Zhang, B., Y. Wu, and Y. Liu, "Wideband single-ended and differential bandpass filters based on terminated coupled line structures," *IEEE Transactions on Microwave Theory and Techniques*, Vol. 65, No. 3, 761–774, Mar. 2017.

[3] Feng, W., W. Che, and Q. Xue, "Balanced filters with wideband common mode suppression using dual-mode ring resonators," *IEEE Transactions on Circuits and Systems I-Regular Papers*, Vol. 62, No. 6, 1499–1507, Jun. 2015.

[4] Li, Z., F. Wei, B. Liu, and X. W. Shi, "Design of balanced wideband BPF based on tri-mode slotline resonators," *IEEE Transactions on Circuits and Systems II-Express Briefs*, Vol. 69, No. 6, 2767–2771, Jun. 2022.

[5] Feng, W., X. Gao, W. Che, W. Yang, and Q. Xue, "High selectivity wideband balanced filters with multiple transmission zeros," *IEEE Transactions on Circuits and Systems II-Express Briefs*, Vol. 64, No. 10, 1182–1186, Oct. 2017.

[6] Pednekar, P. H., W. Hallberg, C. Fager, and T. W. Barton, "Analysis and design of a Doherty-like RF-input load modulated balanced amplifier," *IEEE Transactions on Microwave Theory and Techniques*, Vol. 66, No. 12, 5322–5335, Dec. 2018.

[7] He, D., M. Yu, J. Li, and Z. Yu, "An 18-50-GHz double-balanced Gaas mixer using novel ultrawideband balun," *IEEE Microwave and Wireless Technology Letters*, Vol. 33, No. 6, 723–726, Jun. 2023.

[8] Zhang, G., Q. Zhang, Q. Liu, W. Tang, and J. Yang, "Design of a new dual-band balanced-to-balanced filtering power divider based on the circular microstrip patch resonator," *IEEE Transactions on Circuits and Systems II-Express Briefs*, Vol. 68, No. 12, 3542–3546, Dec. 2021.

[9] Li, H.-Y., J.-X. Xu, and X. Y. Zhang, "Miniaturized balanced filtering power dividers with arbitrary power division ratio using multimode dielectric resonator in single cavity," *IEEE Transactions on Circuits and Systems II-Express Briefs*, Vol. 69, No. 6, 2707–2711, Jun. 2022.

[10] Xia, B., L.-S. Wu, S.-W. Ren, and J.-F. Mao, "A balanced-to-balanced power divider with arbitrary power division," *IEEE Transactions on Microwave Theory and Techniques*, Vol. 61, No. 8, 2831–2840, Aug. 2013.

[11] Wu, L.-S., Y.-X. Guo, and J.-F. Mao, "Balanced-to-balanced Gysel power divider with bandpass filtering response," *IEEE Transactions on Microwave Theory and Techniques*, Vol. 61, No. 12, 4052–4062, Dec. 2013.

[12] Yadav, A. N. and R. Bhattacharjee, "Balanced to unbalanced power divider with arbitrary power ratio," *IEEE Microwave and Wireless Components Letters*, Vol. 26, No. 11, 885–887, Nov. 2016.

[13] Feng, W., M. Hong, M. Xun, and W. Che, "A novel wideband balanced-to-unbalanced power divider using symmetrical transmission lines," *IEEE Microwave and Wireless Components Letters*, Vol. 27, No. 4, 338–340, Apr. 2017.

[14] Huang, F. and L. Zhu, "Balanced-to-unbalanced filtering in-phase power divider based on 2-D patch resonator," *IEEE Microwave and Wireless Technology Letters*, Vol. 33, No. 4, 399–402, Apr. 2023.

[15] Gao, X., W. Feng, W. Che, and Q. Xue, "Wideband balanced-to-unbalanced filtering power dividers based on coupled lines," *IEEE Transactions on Microwave Theory and Techniques*, Vol. 65, No. 1, 86–95, Jan. 2017.

[16] Zhuang, Z., Y. Wu, L. Jiao, W. Wang, and Y. Liu, "Wideband balanced-to-unbalanced filtering unequal power divider with wide stopband and isolation," *Electronics Letters*, Vol. 53, No. 13, 892–893, Jun. 2017.

[17] Xu, K., J. Shi, L. Lin, and J.-X. Chen, "A balanced-to-unbalanced microstrip power divider with filtering function," *IEEE Transactions on Microwave Theory and Techniques*, Vol. 63, No. 8, 2561–2569, Aug. 2015.

[18] Qiu, L.-F., L.-S. Wu, W.-Y. Yin, and J.-F. Mao, "Absorptive bandstop filter with prescribed negative group delay and bandwidth," *IEEE Microwave and Wireless Components Letters*, Vol. 27, No. 7, 639–641, Jul. 2017.

[19] Luo, C., S.-W. Wong, J.-Y. Lin, Y. Yang, Y. Li, X.-Z. Yu, L.-P. Feng, Z.-H. Tu, and L. Zhu, "Quasi-reflectionless microstrip bandpass filters using bandstop filter for out-of-band improvement," *IEEE Transactions on Circuits and Systems II-Express Briefs*, Vol. 67, No. 10, 1849–1853, Oct. 2020.

[20] Gomez-Garcia, R., J.-M. Munoz-Ferreras, and D. Psychogiou, "Dual-behavior resonator-based fully reconfigurable input reflectionless bandpass filters," *IEEE Microwave and Wireless Components Letters*, Vol. 29, No. 1, 35–37, Jan. 2019.

[21] Gomez-Garcia, R., J.-M. Munoz-Ferreras, and D. Psychogiou, "RF reflectionless filtering power dividers," *IEEE Transactions on Circuits and Systems II-Express Briefs*, Vol. 66, No. 6, 933–937, Jun. 2019.

[22] Lce, B., S. Nam, and J. Lee, "Filtering power divider with reflectionless response and wide isolation at output ports," *IEEE Transactions on Microwave Theory and Techniques*, Vol. 67, No. 7, 2684–2692, Jul. 2019.

[23] Zhu, Y.-H., J. Cai, Y. Cao, and J.-X. Chen, "Compact wideband absorptive filtering power divider with a reused composite T-shape network," *IEEE Transactions on Circuits and Systems II-Express Briefs*, Vol. 70, No. 3, 899–903, Mar. 2023.

[24] Lee, B., J. Lee, G. Lee, and J. Lee, "All-port-reflectionless narrowband filtering power divider topology with generic equations," *IEEE Transactions on Circuits and Systems I-regular Papers*, Vol. 69, No. 4, 1417–1426, Apr. 2022.

[25] Zysman, G. I. and A. K. Johnson, "Coupled transmission line networks in an inhomogeneous dielectric medium," *IEEE Transactions on Microwave Theory and Techniques*, Vol. MT17, No. 10, 753–759, 1969.

[26] Velázquez-Ahumada, M., J. Martel, and F. Medina, "Parallel coupled microstrip filters with floating ground-plane conductor for spurious-band suppression," *IEEE Transactions on Microwave Theory and Techniques*, Vol. 53, No. 5, 1823–1828, May 2005.